

LINEAR AND NON-LINEAR OPTIMIZATION OF THE PS2 NEGATIVE MOMENTUM COMPACTION LATTICE

H. Bartosik, Y. Papaphilippou, CERN, Geneva, Switzerland

Abstract

PS2 is a design study of a conventional magnet synchrotron considered to replace the existing PS at CERN. In this paper, studies on different aspect of single particle dynamics in the nominal PS2 Negative Momentum Compaction lattice are described. The global tuning flexibility of the ring and the geometric acceptance is demonstrated by a systematic scan of quadrupole settings. Frequency map analysis and dynamic aperture plots for two different chromaticity correction schemes are presented. The impact of magnet misalignments on the dynamic aperture is studied for one of them. A first study of the beam dynamics with magnetic multipole errors using frequency maps and the corresponding analytical tune-spread footprints is reported. It is thus demonstrated that multipole errors determine to a large extend the beam dynamics in PS2.

INTRODUCTION

A possible upgrade scenario of the CERN injector complex considers the aging PS to be replaced by a separated function synchrotron called PS2. As the PS2 lattice is designed with negative momentum compaction (NMC), the transition energy γ_t is imaginary, thus allowing operational flexibility and reducing beam losses during acceleration. The PS2 should provide the same flexibility for handling different kind of beams as the PS but with higher intensity. Since the intensity of the proton beam will be roughly doubled with respect to the PS, the injection energy is increased from 1.4 GeV to 4 GeV for obtaining similar space charge induced incoherent tune shift. The extraction energy is increased to 50 GeV, which would allow a further reduction of beam instabilities due to collective effects in the subsequent SPS. In order to achieve an optimized filling pattern of the SPS for delivering LHC bunch trains, the circumference of the PS2 is fixed to 1346.4 m, i.e. 15/77 of the circumference of the SPS. A summary of the main lattice design constraints is given in Table 1.

Table 1: PS2 Lattice Design Constraints

Parameter	Value
Injection energy, kinetic	4 GeV
Extraction energy, kinetic	50 GeV
Circumference	1346.4 m
Transition energy	imaginary
Maximum bending field	1.7 T
Maximum quadrupole gradient	16 T/m
Minimum drift space, dipoles / quads	0.8 / 1.3 m

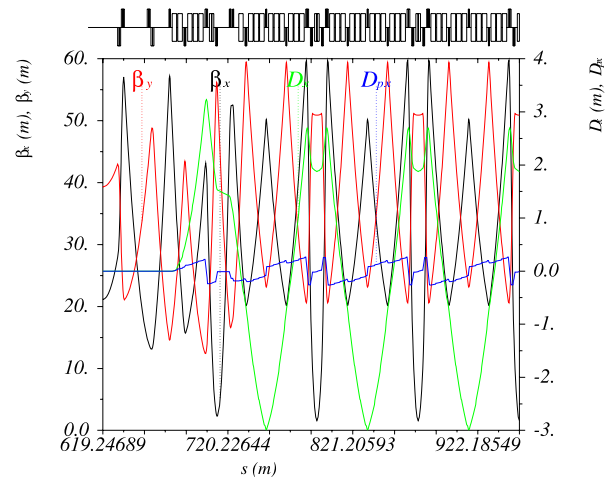


Figure 1: Optics functions for a quarter of the PS2 lattice, with $(Q_x, Q_y) = (11.81, 6.71)$ and $\gamma_t = 25.3i$.

The baseline lattice for the PS2 [1] has a twofold symmetry with tunable arcs and two zero dispersion long straight sections (LSS). Each of the arcs consists of five NMC cells and two dispersion suppressor modules. The working point of the machine is tuned by adjusting the phase advances in the NMC cells and matching the dispersion suppressors to the optics of the LSSs. The mirror symmetric LSSs are based on two pairs of quadrupole doublets [2] formed by wide aperture magnets with a length of 2.4 m. As required by the general layout of the LHC injector complex, all beam transfer systems are installed at the same LSS. The layout of the NMC cell is based on two FODO cells, linked by a central insertion of quadrupole doublets. Imposing negative dispersion at the entrance of the module leads to negative momentum compaction [3]. Optimizing to maximum gradients of 16 T/m yields 3 types of quadrupoles for the 4 families with lengths of 0.8 m, 1.6 m and 2.2 m. The dispersion suppressor modules on either side of the NMC arc share their first and last quadrupole with the adjacent LSS and NMC cell, respectively. Ten dipole magnets and 6 independent quadrupole families based on the same types of magnets as used in the arc cells are needed to achieve the matching constraints. The PS2 lattice contains 170 dipoles with a length of 3.7 m and a maximum field of 1.7 T at top energy. The 116 quadrupole magnets are grouped to 15 families. They are based on 4 different types, 3 for the arcs and the wide aperture magnets for the LSSs.

Figure 1 shows the optics functions for the working point $(Q_x, Q_y) = (11.81, 6.70)$ with $\gamma_t = 25.3i$. The natural chromaticities of $(\xi_x, \xi_y) = (-21.5, -11.0)$ are compensated by relatively weak sextupoles, as they are located at high-dispersion areas.

TUNING FLEXIBILITY

The working point is tuned by changing the phase advances of the basic NMC cell and matching the dispersion suppressor module to the LSS injection optics. A complete picture of the achievable tuning range is obtained from a Global Analysis of all Stable Solutions (GLASS) [4]. In the present case, basically the 4 quadrupole families of the NMC module determine the tune. Thus, a four dimensional parameter space has to be explored. The normalized gradients are scanned in steps of 0.001 m^{-2} , i.e. a total of 10^8 possible combinations. For each stable solution, the geometrical acceptance is computed using the fixed target beam parameters at injection, i.e. normalized emittances of $(\epsilon_x, \epsilon_y) = (9, 6) \pi \text{ mm.mrad}$, and momentum spread of $\delta p/p = 0.65\%$. In addition, 20% β -beat and 5% parasitic dispersion are assumed. These values are pessimistic compared to the values observed in the chromaticity and orbit correction studies on the same lattice [5]. For each of these solutions, the main parameters of the ring together with all quadrupole gradients are stored. Finally, all valid solutions are obtained by filtering the solutions where the quadrupole gradients in the suppressor module are below 16 T/m without changing sign and the number of beam sizes N_σ accepted by the vacuum chamber is at least 3.3.

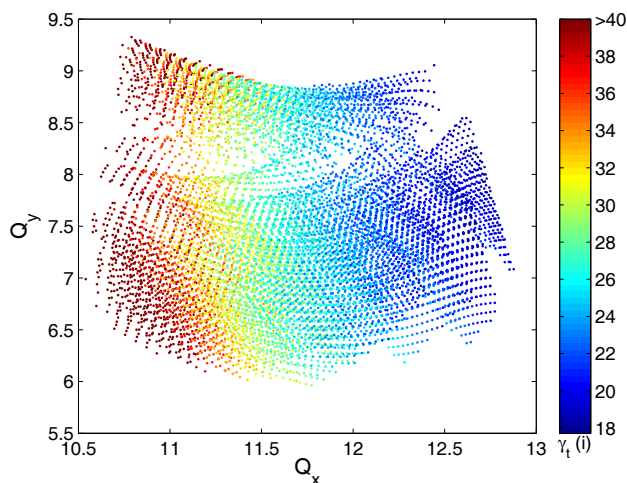


Figure 2: Optics solutions for the nominal PS2 lattice. The color-code indicates the value of γ_t as function of the betatron tunes, with values above $40i$ represented by dark red.

One of the interesting parameters changing with the tune is the transition energy γ_t . Figure 2 shows γ_t for all solutions in the tune diagram. The smaller tuning range in the horizontal plane and the clear dependence of γ_t on the horizontal tune can be explained by the constraint of periodicity of the dispersion function, which reduces the number of possible solutions and the flexibility in γ_t . The smallest reachable value of $\gamma_t = 18i$ is obtained for $Q_x \approx 12.5$ while γ_t goes up to $80i$ for tunes around $Q_x \approx 10.5$. It should be emphasized however that γ_t can be adjusted by a few units for most of the working points, as different sets of solutions are found for a given region in the tune diagram.

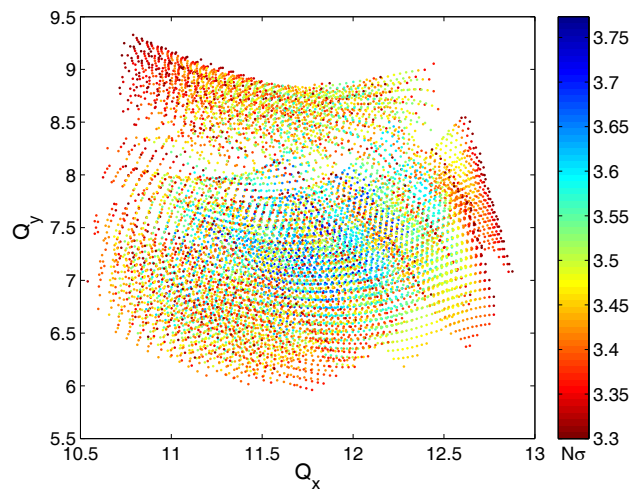


Figure 3: PS2 tuning range, color-coded with the geometrical acceptance in terms of high-intensity beam sizes.

Figure 3 shows the geometrical acceptance N_σ of the machine, i.e. the number of beam sizes fitting into the vacuum chamber, as a function of the betatron tunes. A large number of solutions is found with a maximal geometrical acceptance between 3.3σ and 3.5σ . Higher geometrical acceptance is achieved for solutions in the center of the tuning range with peak values of 3.8σ . Note that for the nominal working point $N_\sigma = 3.6$.

CHROMATICITY CORRECTION

Chromaticity control is enabled through sextupole magnets with a length of 40 cm located in dispersive regions of the arcs. In order to minimize their contribution to non-linear effects, chromatic sextupoles are preferably positioned in high dispersive areas of the ring where the β -functions reach maximal values, i.e. close to the quadrupoles in the arc cells. Previous studies showed [5]

Table 2: Chromaticity Correcting Sextupole Schemes

Scheme	Hor. correctors	Vert. correctors
2 families	24 MS.2	24 MS.3
4 families	24 MS.2, 12 MS.4	24 MS.3, 24 MS.1

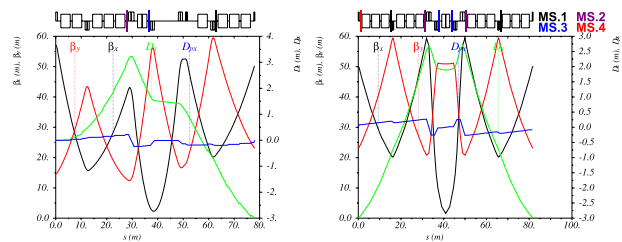


Figure 4: Chromaticity correction sextupoles in the dispersion suppressor (left) and the basic NMC cell (right) of the PS2 ring. The color-code represents the different families.

that it is advantageous to extend the sextupole families distributed in the NMC cells by additional members in the dispersion suppressors for minimizing off-momentum β -beat. Two different configurations of sextupoles are considered (Fig. 4 and Table 2). The two family (extended) scheme is formed by 48 magnets, where 4 sextupoles are installed symmetrically around the quadrupole doublets in each NMC cell. Together with the 8 additional members in the dispersion suppressor modules, they form the families MS.2 and MS.3. The four family (extended) scheme requires 84 sextupoles. Twenty additional sextupoles are installed close to the central quadrupole in the NMC cell. They are connected in series with four sextupoles in the suppressors, to form the third family MS.1. The 12 magnets of the fourth family MS.4 are located in the NMC modules at mirror symmetric positions with respect to the center of the arc. Note that, in contrast to previous versions described in [5], all the families apart from MS.4 are extended in the dispersion suppressor cells, as this leads to smoother off-momentum optics.

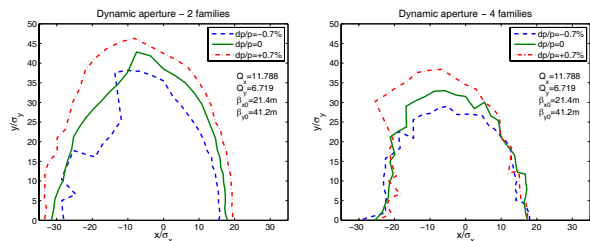


Figure 5: Dynamic aperture for the ideal PS2 lattice including fringe fields for the two (left) and the four family scheme with reduced second order chromaticity (right).

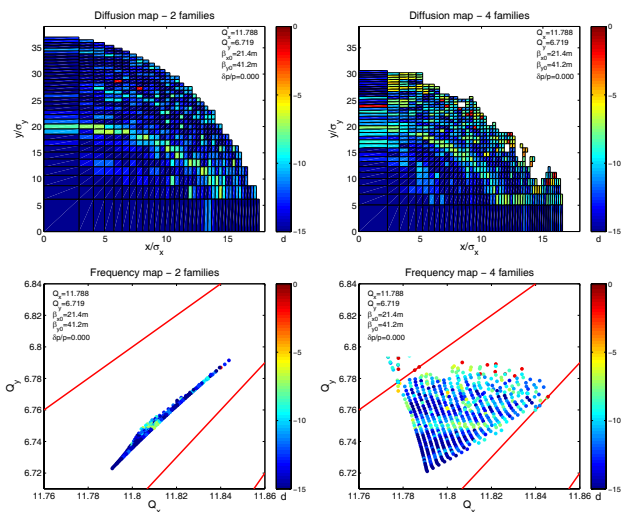


Figure 6: Diffusion and Frequency Maps for the two (left) and four (right) families schemes. The colormap shows the diffusion coefficient. Systematic resonances up to 6^{th} order are shown in the frequency maps.

First order chromaticity can be set to zero with each of the two correction schemes. Second order chromaticity and linear tune-shift with amplitude can be controlled to some extent with the 4 family scheme. The dynamic aperture is studied for the error-free lattice including fringe field effects by tracking particles for 1000 turns. Compared to the geometrical acceptance, the area of stable particle motion is huge for both schemes, as shown in Fig. 5. Beam size values quoted here correspond to the fixed target beam at injection, at which the geometrical acceptance in the arcs is around $N_\sigma = 3.6$. Frequency maps [6] for on-momentum particles are presented in Fig. 6 for both sextupole schemes. The additional sextupoles in the four family scheme change the tune foot-print which leads to a smaller dynamic aperture for the working point studied here. However, for other working points, the additional families allow to reshape the footprint which may result in an increased dynamic aperture. As for the dynamic aperture scans, the working point used for these frequency map studies is optimized in terms of dynamic aperture with respect to single particle dynamics in the error-free lattice.

MAGNET MISALIGNMENTS

Correction of orbit distortion in the PS2 is achieved by 108 bi-planar beam position monitors (BPMs) in combination with 60 correctors for the vertical plane and 48 for the horizontal plane located close to quadrupole magnets. The effect of random magnet errors on closed orbit distortion is studied for the following machine imperfections: misalignment of dipole, quadrupole and sextupole magnets with a Gaussian distribution cut at 3σ and errors in the main field component of dipoles and quadrupoles with a cut at 2σ . The corresponding rms values for the 100 error seeds are summarized in Table 3. In addition, random misalignments with a flat distribution of values between ± 0.5 mm are assigned to the BPMs.

Table 3: Assumed Machine Imperfections for the 100 Error Seeds (Rms Values)

Type	Dipole	Quadr.	Sext.
Relative field error	$5 \cdot 10^{-4}$	$5 \cdot 10^{-4}$	0
Transverse shift (mm)	0.3	0.2	0.2
Longitudinal shift (mm)	1	1	1
Tilt (mrad)	0.3	0.3	0.3

The maximal deviation from the nominal orbit before and after the correction in the lattice with the two family sextupole scheme is shown in Fig. 7. In all cases, the maximum orbit distortion can be reduced well below 1 mm in both planes. Maximal corrector kicks of up to 0.4 mrad are needed in some of the cases. As already shown in previous studies [5], the β -beat resulting from magnet misalignments and random errors in the main components of the linear magnets are reduced to below 10% by the orbit correction. Therefore, no additional measures seem neces-

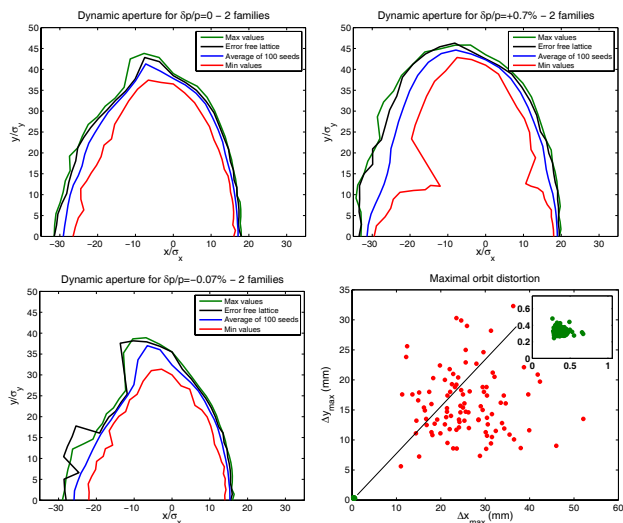


Figure 7: Impact of machine imperfections for a sample of 100 seeds in the case of the two family sextupole scheme: dynamic aperture scans for $\delta p/p = 0$ and $\pm 0.7\%$, together with the distribution of the maximum orbit distortion before and after correction.

sary for restoring the optical functions' variation. Figure 7 shows also the impact of the errors for the 100 seeds on the dynamic aperture. The maximal, average and minimal dynamic aperture together with the dynamic aperture for the error-free lattice are plotted in green, blue, red and black, respectively. In all cases, the dynamic aperture is slightly reduced but still remains comfortable. The biggest reduction is observed for positive momentum spread.

MAGNETIC MULTIPOLE ERRORS

A first study on the impact of multipole errors on the beam dynamics including tune-shift with amplitude and FMA is based on error tables from existing machines. In particular, the measured multipole components of the J-PARC Main Ring (MR) magnets at 20 GeV beam energy [7] served as example for the quadrupoles and sextupoles. For the dipoles on the other hand, the multipole errors from the Fermilab Main Injector [8] at injection energy are considered. The field distribution of the dipoles calculated from these multipole components provides a good field region of around 60 mm (the horizontal half-aperture in PS2 dipoles is 63 mm), which is similar to the J-PARC dipoles at 3 GeV [9]. At this stage, only upright components of multipole errors are included in the simulations.

The first step in the simulations is assigning the machine imperfections to the magnets, i.e. misalignments together with the systematic and random multipole errors (Gaussian distributions cut at 2σ) according to Table 3 and Table 4. After orbit correction, the tune of the machine is readjusted using the 2 central quadrupole families of the NMC module. Chromaticity is reset to zero with the 2 main sextupoles families. Using this lattice, particles are tracked for

1056 turns in 5D. At the same time, the tune shift with amplitude coefficients (anharmonicities) of the normal form analysis are calculated up to 5^{th} order. Figure 8 shows the results for one error seed and momentum deviations of $\delta p/p = 0$ and $\pm 0.7\%$. Compared to the error-free lattice with the 2 family sextupole scheme (cf. Fig. 6), a strong degradation of the stable area in configuration space is observed. The most severe reduction occurs for negative momentum offset, where the dynamic aperture is limited by the difference coupling resonance and reduced to below 3σ of the fixed target beam, i.e. below the physical aperture. In contrast to that, the limiting resonances for positive momenta are found above the working point. The reason for this can be understood with the frequency map analysis: For positive momentum offset the tune shift with amplitude leads to increasing betatron-tunes. On the other hand negative tune shift with amplitude is observed for negative momentum offset. Thus, the orientation of the tune-footprint changes completely and strong folding is observed for on-momentum particles. The dominant anharmonicity terms are of higher order which results in large tune-shift for increasing amplitude and the folding of the frequency maps. Both effects can be reconstructed in good agreement from the anharmonicities up to 5^{th} order (cf. Fig. 8).

The biggest contribution to the non-linear tune-shift with amplitude and to dynamic aperture reduction is due to the higher order components of the dipoles, particularly due to their large number. In addition, the dipoles are relatively strong compared to the quadrupoles and especially to the sextupoles. Therefore, multipole components with similar relative strength have much bigger absolute values for the dipoles. Although the full width of the vacuum chamber lies within the good field region of the dipoles for the assumed multipole distribution, the impact on the particle motion is severe. Since the excitation of the sextupoles needed for chromaticity correction is relatively small, the high order multipole errors determine to a large extend the non-linear single particle dynamics in the PS2 lattice.

Table 4: Assumed Relative Multipole Components in Units of 10^{-4} at the Respective Reference Radius R

Order n	Dipole b_n/b_1 (R=2.54 cm)	Quadrupole b_n/b_2 (R=5.95 cm)	Sextupole b_n/b_3 (R=5.95 cm)
1	$10^4 \pm 5$	± 1	± 3
2	0.06 ± 0.23	$10^4 \pm 5$	± 10
3	-0.4 ± 0.2	-2 ± 1	$10^4 \pm 5$
4	0.04 ± 0.08	1 ± 1	-0.5 ± 1.5
5	0.33 ± 0.08	1 ± 1.5	0.5 ± 1.5
6	-0.01 ± 0.08	3 ± 1	-1 ± 0.5
7	-0.03 ± 0.1	0.5 ± 1	1 ± 0.5
8	-	0.5 ± 0.5	0.5 ± 0.5
9	-	0.1 ± 0.3	-4 ± 0.3
10	-	0.5 ± 0.3	0.1 ± 0.5
11	-	0.1 ± 0.3	0.1 ± 0.5

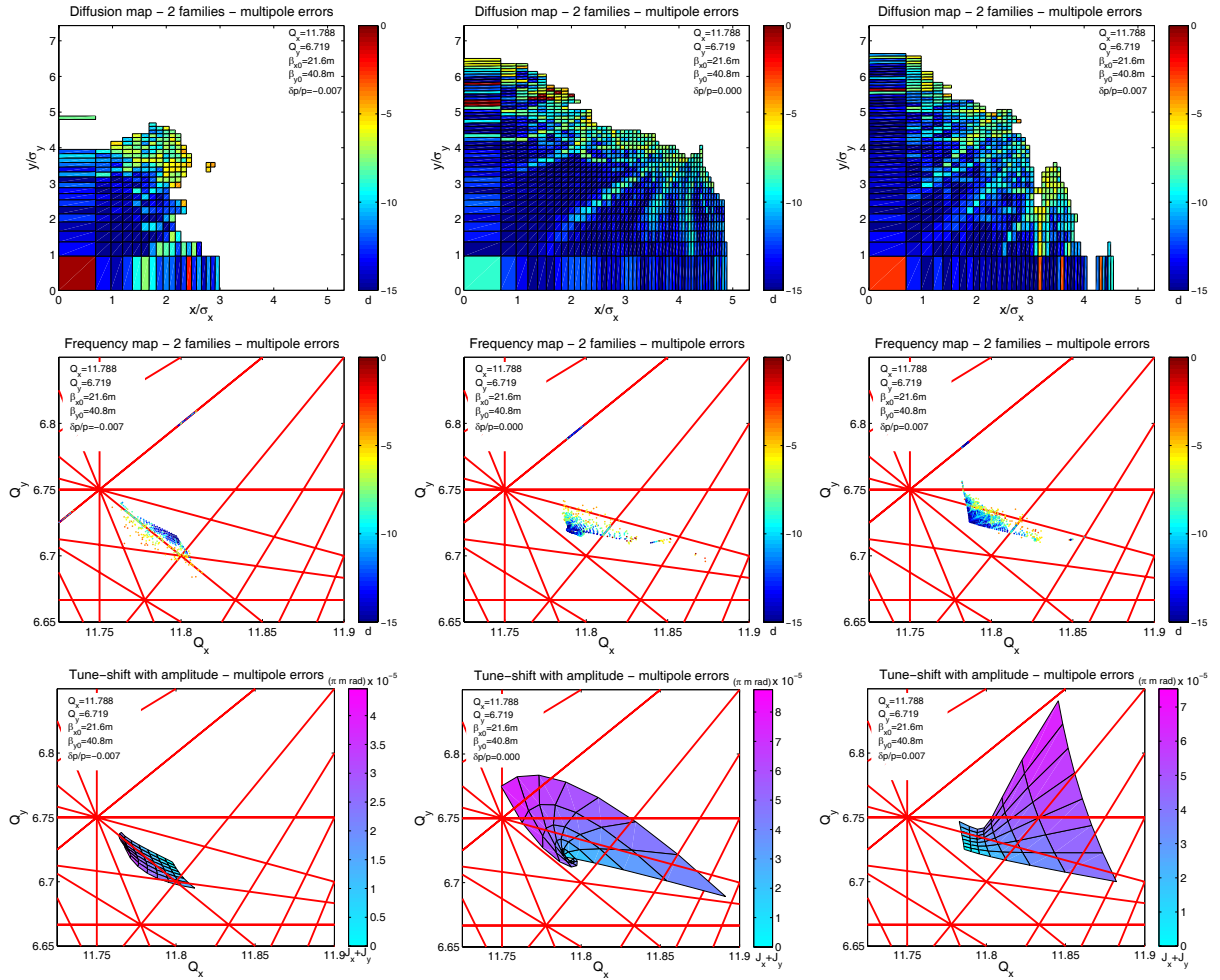


Figure 8: Diffusion map, frequency maps and tune-shift with amplitude reconstructed from anharmonicities up to 5^{th} order for $\delta p/p = 0$ and $\pm 0.7\%$ for the PS2 lattice (two family sextupole scheme) including magnet misalignments and multipole errors for one error seed sample. The tune diagrams show systematic resonances up to 8^{th} order.

CONCLUSION

In conclusion, the PS2 negative momentum compaction lattice provides high tuning flexibility. Chromaticity correction can be achieved with a two and a four families scheme of relatively weak sextupoles. Orbit distortion and β -beat induced by magnet misalignments and random errors in the main components of the linear magnets can be reduced to tolerable values and their effect on the dynamic aperture is moderate. On the other hand, first studies show significant impact of multipole errors on the beam dynamics with a strong reduction of the dynamic aperture. In fact, the non-linear single particle motion is completely dominated by the high order multipoles (mainly of the dipoles) leading to strong non-linear tune shift with amplitude. Further studies are needed for establishing an error table which allows for sufficient (off-momentum) dynamic aperture. In particular, the individual contributions of the high order multipole components of the dipoles have to be understood. The final choice of the working point should be based on

space charge simulations including multipole errors. Additional correction schemes may also be considered.

REFERENCES

- [1] H. Bartosik et al., THPE022, proceedings of the International Particle Accelerator Conference 2010.
- [2] W. Bartmann et al., THPEB028, proceedings of the International Particle Accelerator Conference 2010.
- [3] S. Y. Lee, K. Y. Ng and D. Trbojevic, Phys. Rev. E 48 (1993).
- [4] D. S. Robin et al., Phys. Rev. ST Accel. Beams 11 (2008).
- [5] H. Bartosik et al., THPE023, proceedings of the International Particle Accelerator Conference 2010.
- [6] J. Laskar, proceedings of the 2003 Particle Accelerator Conference, and references therein.
- [7] K. Niki et al., WEPCH028, proceedings of the European Particle Accelerator Conference 2006.
- [8] Fermilab Main Injector, RUN II handbook.
- [9] J-PARC, technical design report, 2003.